SANDIA REPORT
SAND2009-0239
Unlimited Release
Printed January 2009

Investigation of Biologically-Designed Metal-Specific Chelators for Potential Metal Recovery and Waste Remediation Applications

Louise J. Criscenti and Nathan W. Ockwig

Prepared by
Sandia National Laboratories
Albuquerque, New Mexico 87185 and Livermore, California 94550

Sandia is a multiprogram laboratory operated by Sandia Corporation,
a Lockheed Martin Company, for the United States Department of Energy's
National Nuclear Security Administration under Contract DE-AC04-94AL85000.

Issued by Sandia National Laboratories, operated for the United States Department of Energy by Sandia Corporation.

Available to DOE and DOE contractors from
U.S. Department of Energy
Office of Scientific and Technical Information
P.O. Box 62
Oak Ridge, TN 37831

Telephone:	(865) 576-8401
Facsimile:	(865) 576-5728
E-Mail:	reports@adonis.osti.gov
Online ordering:	http://www.osti.gov/bridge

Available to the public from
U.S. Department of Commerce
National Technical Information Service
5285 Port Royal Rd.
Springfield, VA 22161

Telephone:	(800) 553-6847
Facsimile:	(703) 605-6900
E-Mail:	orders@ntis.fedworld.gov
Online order:	http://www.ntis.gov/help/ordermethods.asp?loc=7-4-0#online

SAND2009-0239
Unlimited Release
Printed January 2009

Investigation of Biologically-Designed Metal-Specific Chelators for Potential Metal Recovery and Waste Remediation Applications

Louise J. Criscenti and Nathan W. Ockwig
Geochemistry Department
Sandia National Laboratories
P.O. Box 5800
Albuquerque, New Mexico 87185-MS0754

Abstract

Bacteria, algae and plants produce metal-specific chelators to capture required nutrient or toxic trace metals. Biological systems are thought to be very efficient, honed by evolutionary forces over time. Understanding the approaches used by living organisms to select for specific metals in the environment may lead to design of cheaper and more effective approaches for metal recovery and contaminant-metal remediation. In this study, the binding of a common siderophore, desferrioxamine B (DFO-B), to three aqueous metal cations, Fe(II), Fe(III), and UO_2(VI) was investigated using classical molecular dynamics. DFO-B has three acetohydroxamate groups and a terminal amine group that all deprotonate with increasing pH. For all three metals, complexes with DFO-B (-2) are the most stable and favored under alkaline conditions. Under more acidic conditions, the metal-DFO complexes involve chelation with both acetohydroxamate and acetylamine groups. The approach taken here allows for detailed investigation of metal binding to biologically-designed organic ligands.

ACKNOWLEDGMENTS

We would like to thank Jeffery A. Greathouse for providing us with the force field parameter set for uranyl and Randall T. Cygan for reviewing this report.

Funding for this project cam e from Sandia Nationa l Laboratories Laboratory Directed Research Program (LDRD) through the Energy, Resources and Nonproliferation Strategic Managem ent Unit.

CONTENTS

FIGURES

TABLES

1. INTRODUCTION

New techniques are necessary for economic metal recovery and metal-waste remediation. Bacteria, algae and plants produce metal-specific chelators to capture required nutrient or toxic trace metals. Biological systems are thought to be very efficient, honed by evolutionary forces over time. Understanding the approaches used by living organisms to select for specific metals in the environment will allow us to design cheaper and more effective approaches for metal recovery and contaminant-metal remediation. Bacteria and algae produce siderophores that capture life-supporting trace metals. The metal-siderophore complexes are adsorbed by the parent cell which then extracts the metal for its use. Plants produce phytochelatins to bind and eliminate toxic trace metals. Siderophores were first recognized for their ability to bind Fe(III); however, they also bind other metal cations: the 1:1 formation constants of Ca, Al, and Fe(III) to a common siderophore desferrioxamine B (DFO-B) are 10^{2}, 10^{24}, and $10^{30.7}$ (Hernlem et al., 1999). In addition, siderophores form very strong complexes with the actinides; the 1:1 formation constant for DFO-B:Pu(IV) is $10^{30.8}$. In the last few years, experiments have shown that siderophore-producing bacteria can leach uranium from crushed mill tailings, enhance the dissolution of solid UO_2 (Frazier et al., 2005), and remove adsorbed uranyl complexes from kaolinite surfaces, thereby potentially mobilizing actinides in the environment. Phytochelatins also complex many important trace metals such as arsenic, selenium, lead, and cadmium. Both types of metal chelators (i.e., siderophores and phytochelatins) have primarily been studied through field observation and batch or column experiments. For the most part, the stoichiometries and structures of the metal (M)-chelate (C) species formed (e.g., MC, M_2C, MC_2), the impact of pH and solution composition, and the binding mechanisms and constants have not been firmly established. With more quantitative analysis, these chelators, produced by organisms to cope with metal-specific needs, could provide the foundation for more effective metal recovery and waste remediation.

Siderophores are common in soil and marine environments (0.1 – 0.01 μM in soils). They solubilize Fe-hydroxides and maintain soluble iron concentration at an optimal domain for cell growth (Boukhalfa and Crumbliss, 2002). They selectively acquire and mediate iron transport and deposition inside the cell. Almost 500 compounds are identified as siderophores which are defined as low molecular weight organic chelators with a very high and specific affinity for Fe(III). They usually include hydroxamate, catecholate, and carboxylic acid functional groups (Boukhalfa et al., 2007). These binding groups, rich in hard O donors, have large affinities for Fe(III). Most siderophores are hexadentate and fully coordinate Fe(III) to form 1:1 Fe(III)/siderophore complexes.

We have chosen to study DFO-B because of its ubiquity in natural environments. DFO-B has four protonation constants, one for each of three acetohydroxamate groups and one for a terminal amine group. The structure of DFO-B is discussed in detail in Section 2. Table 1 lists some of the reported association constants for heavy metal and actinide chelation to DFO-B. Research programs focused on the interaction of DFO-B or modified versions of DFO-B with actinides have grown both to evaluate its use for plutonium chelation (Boukhalfa et al., 2007) and its ability to increase the dissolution of iron oxides and UO_2 (Frazier et al., 2005).

To date, classical molecular dynamics (MD) simulations of siderophores or phytochelatins have not been published. In this report, the binding of three metal cations Fe(II), Fe(III), and UO_2(VI) to DFO-B is explored through classical molecular simulation techniques. Functional groups of DFO-B will deprotonate as a function of pH. The impact of different DFO-B protonation schemes and net charge on metal-binding are examined.

Table 1. Association Constants for Aqueous Metal-Siderophore Complexes

Metal Ion	DFO-B Species	Log K	Reference
Fe(III)	DFO	30.99	Evers et al. (1989)
UO_2(VI) H	$_2$DFO	22.93	Mullen et al. (2007)
UO_2(VI) HDFO		17.12	
UO_2(VI) OHDFOH		22.76	
Pu(IV) H	$_2$DFO	35.48	Boukhalfa et al. (2007)
Pu(IV) HDFO		34.87	
Pu(IV) DFO		33.98	
Pu(IV) DFO(OH)		27.33	
Th(IV)	DFO	26.6	Whisenhunt et al. (1996)
Zn(II)	DFO	9.55	Hernlem et al. (1996)
Pb(II) DFO		10.00	
Sn(II) DFO		21.14	
Cu(II) DFO		13.73	
Bi(III) DFO		23.5	

2. APPROACH

The approach taken in this study was to investigate the binding of three aqueous metal ions, namely Fe(III), Fe(II), and UO_2(VI), to one common siderophore, desferrioxamine B (DFO-B), that has been reported to have 1:1 binding constants for Ca(II), Al(III), Fe(III), and Pu(IV) of 10^2, 10^{24}, $10^{30.7}$, and $10^{30.8}$, respectively. The fully-protonated structure of DFO-B is given in Figure 1.

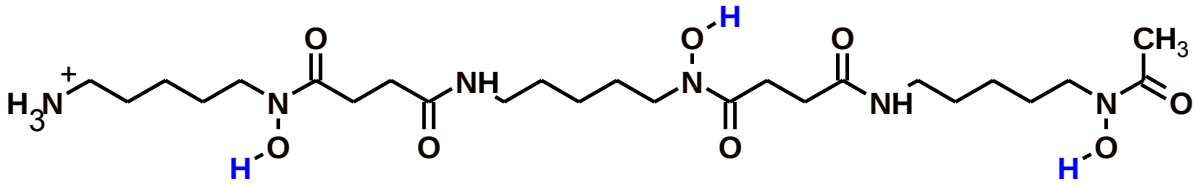

Figure 1. The structure of desferroxamine B.

DFO-B cation has three hydroxamate (-NOH) groups and one amine group ($-NH_3^+$) that deprotonate in alkaline solutions. There are four proton dissociation constants (p K_a) at 8.3, 9.0, 9.46, and 10.84 which correspond to successive deprotonation of the three hydroxamate groups and the amine group respectively (Edwards et al., 2005). Therefore, there are five different charged states of DFO-B referred to simply as DFO in the following equations:

$$H_4DFO^+ \xleftrightarrow{K_1} H_3DFO \xleftrightarrow{K_2} H_2DFO^- \xleftrightarrow{K_3} HDFO^{2-} \xleftrightarrow{K_4} DFO^{3-}$$

where

$$K_1 = \frac{[H_3DFO][H^+]}{[H_4DFO^+]},\ K_2 = \frac{[H_2DFO^-][H^+]}{[H_3DFO]},\ K_3 = \frac{[HDFO^{2-}][H^+]}{[H_2DFO^{1-}]},\ K_4 = \frac{[DFO^{3-}][H^+]}{[HDFO^{2-}]}$$

DFO-B changes charge state over a relatively narrow alkaline pH range, from 8.3 to 10.9, and will be primarily in the positively-charged form H_4DFO^+ at neutral or acid pH (pH < 8.3). The first three constants correspond to the deprotonation of the three hydroxamate groups. The fourth equilibration constant K_4 corresponds to the deprotonation of the terminal amine group. Although there are only five charge states, there are nine possible DFO-B configurations because, for example, a neutral DFO-B ligand can have three different structures depending on which of the three hydroxamate groups deprotonates. Figure 2 illustrates the nine different protonation schemes possible for DFO-B.

Acetohydroxamic acid (aHa) is a smaller molecule that is often chosen to serve as a model for simulating the more complex DFO-B. Studies of aHa have shown that it can exist in either an enol- or keto-form. Theoretical studies indicate that the keto-form is dominant in aqueous solution with the *cis* conformation being more stable than the *trans* conformation (Edwards et al., 2005). These conformations are illustrated in Figure 3. The *cis* keto-form can undergo two

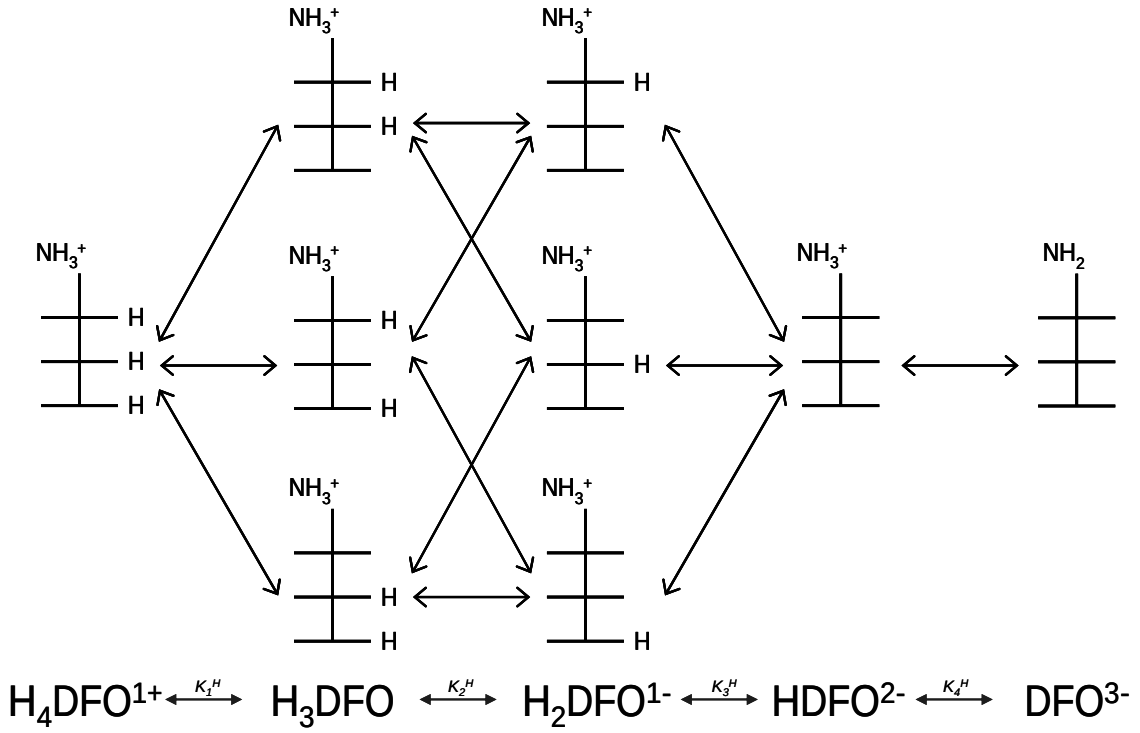

Figure 2. The nine possible configurations of the DFO-B in the five distinct charged states (dependent upon solution pH) and the exchange pathways. Specifically, these are, H_4DFO^{1+}, H_3DFO, H_2DFO^{1-}, and $HDFO^{2-}$ and DFO^{3-}.

types of deprotonation: the nitrogen atom or the oxygen atom in the hydroxamate group can deprotonate. Through infrared, resonance Raman, and UV-vis spectroscopy combined with DFT calculated spectra, Edwards et al. (2005) determined that deprotonation occurs at the oxygen atom in aqueous solutions. The resonance structures associated with the deprotonation of the oxygen atom are illustrated in Figure 3 and are used in our study to construct deprotonated hydroxamate groups in DFO-B.

The complexes formed between each of the nine configurations and the metal ions Fe(III), Fe(II), and UO_2(VI) were modeled to evaluate the relative stability of the metal-ligand complexes as a function of pH. These investigations were performed using classical force field molecular dynamic simulations.

2.1 Classical Force Field Molecular Modeling.

Classical molecular modeling simulations were performed using the Forcite module of the Materials Studio software package (Accelyrs Inc., San Diego) and the consistent-valence force field CVFF (Dauber-Osguthorpe, 1988) supplemented with force field parameter sets for Fe(II), Fe(III) and UO_2(VI). The CVFF force field was fitted to small organic crystals and gas phase structures. The potential energy expression includes terms that represent the energy of bond length deformation, bond angles, torsion angles, and out-of-plane interactions as well as terms to describe Coulombic and van der Waals interactions.

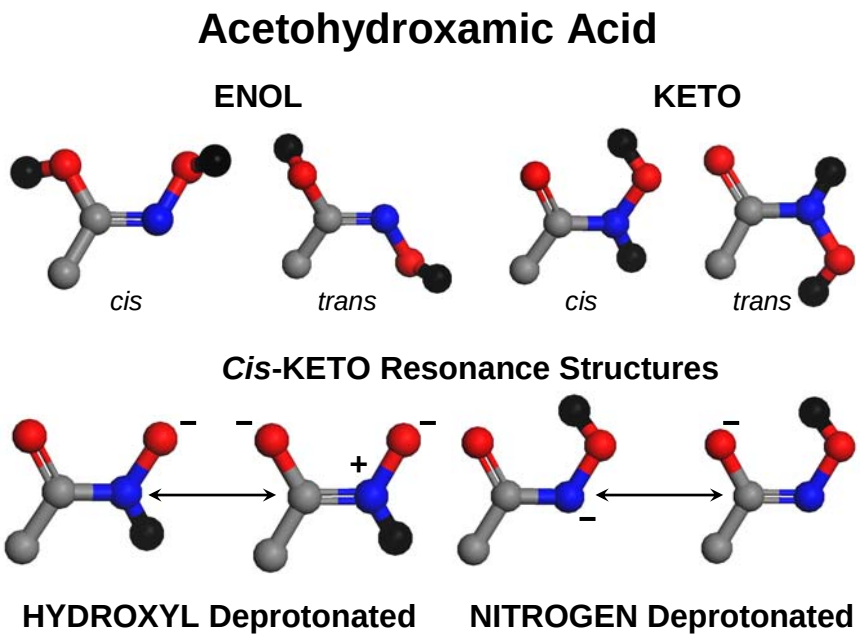

Figure 3. (a) Schematics of acetohydroxamine acid conformers. (b) Two resonance structures associated with deprotonation of cis-keto conformer. Figure after Edwards et al. (2005).

The charges on the siderophore were determined using the bond increment method incorporated in CVFF. Figure 4 illustrates the CVFF atom types used to describe the siderophores and the charges assigned to the atoms of both the acetohydroxamate and terminal amine groups. Atom types and charges change with deprotonation (i.e., compare Figure 4A with Figure 4B).

Force field parameters for Fe(II) and Fe(III) compatible with the CVFF force field have not yet been reported in the literature. However, Curtiss et al. (1987) calculated potentials for Fe^{2+} and Fe^{3+} interacting with H_2O using *ab initio* molecular orbital methods with different basis sets. Curtiss et al. (1987) also fit the *ab initio* Fe-H_2O potentials with empirical expressions of a different form than used in CVFF. These empirical potentials are significantly shallower than the *ab initio* potentials. For this study, the empirical potential curves from Curtiss et al. (1987) were re-fit using the form of the potential used in CVFF:

$$\text{Potential Energy (kcal/mol)} = V(r) = \frac{q_i q_j}{r} + 4\varepsilon\left[\left(\frac{\sigma}{r}\right)^{12} - \left(\frac{\sigma}{r}\right)^{6}\right]$$

where the potential energy is defined as the sum of a Coulombic term and a 12-6 Lennard-Jones term. The parameters in the expression are the charges on the two ions or molecules in the system (q_i, q_j), the distance r between the two species i and j, σ is the finite distance at which the interparticle distance is zero, and, ε is the depth of the potential well. A comparison of Curtiss et al.'s (1987) and our empirical potential curves is provided in Figure 5. These potential curves are very similar; however, it should be noted that the potential wells calculated from the empirical expressions are much shallower than those determined from quantum mechanics. It also should be noted that we used the pair potential parameters provided by Guàrdia and Padró

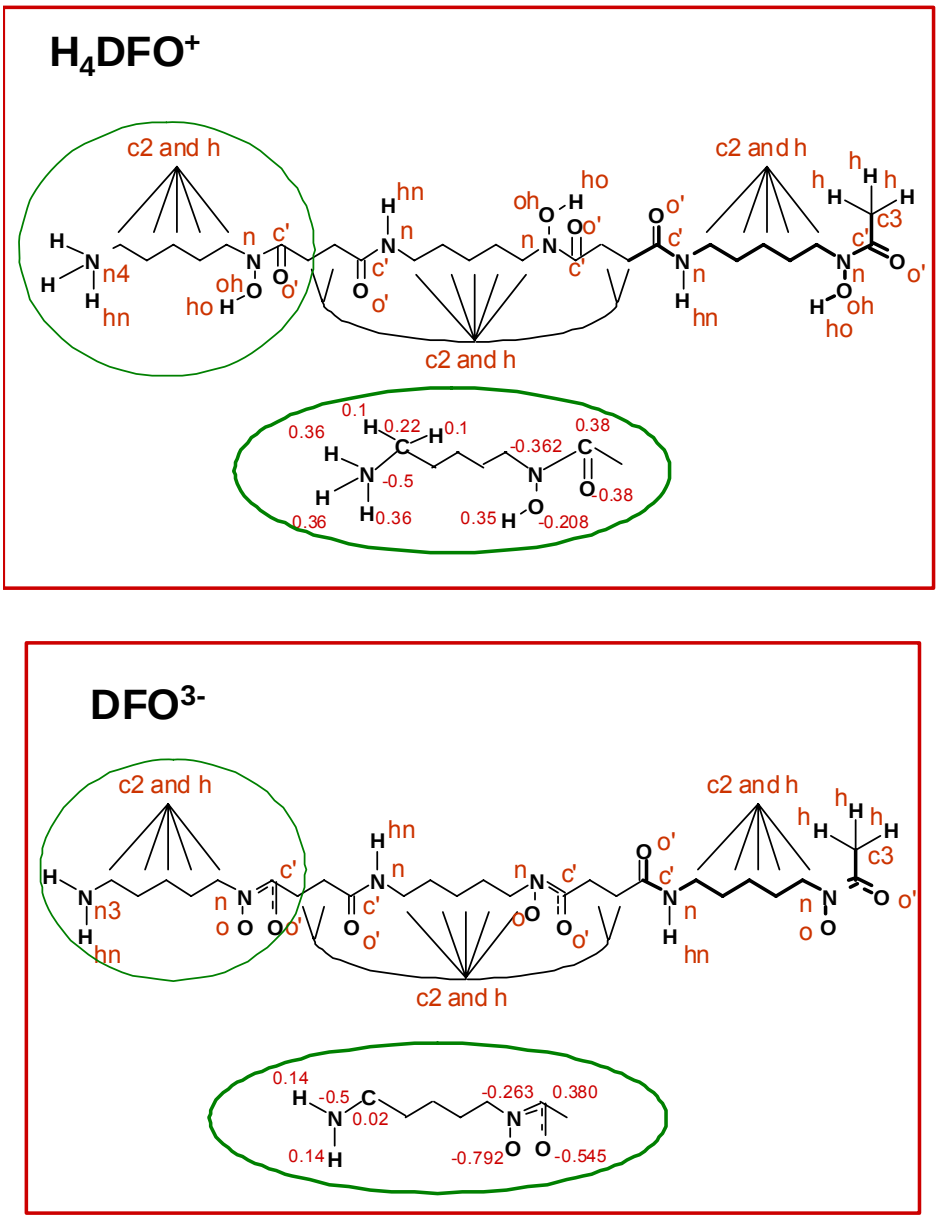

Figure 4. CVFF force field types and charges for H_4DFO^+ and DFO_3^-.

(1990) to reproduce the potentials provided by Curtiss et al. (1987), and this set of parameters does not accurately reproduce the curves illustrated in Curtiss et al.'s (1987) paper. Both of our empirical curves are even shallower than those provided by Curtiss et al. (1987). This discrepancy should be investigated further in future work.

For UO_2(VI), we chose to use the parameter set developed by Guilbaud and Wipff (1996) that also allows for angle-bending and bond-stretching within the polyatomic cation. The Lennard-Jones parameters used for UO_2(VI), Fe(II), and Fe(III) are provided in Table 1.

Molecular dynamics simulations were performed to study metal-siderophore complexation in vacuum. Each of the siderophore configurations illustrated in Figure 2 was geometry optimized.

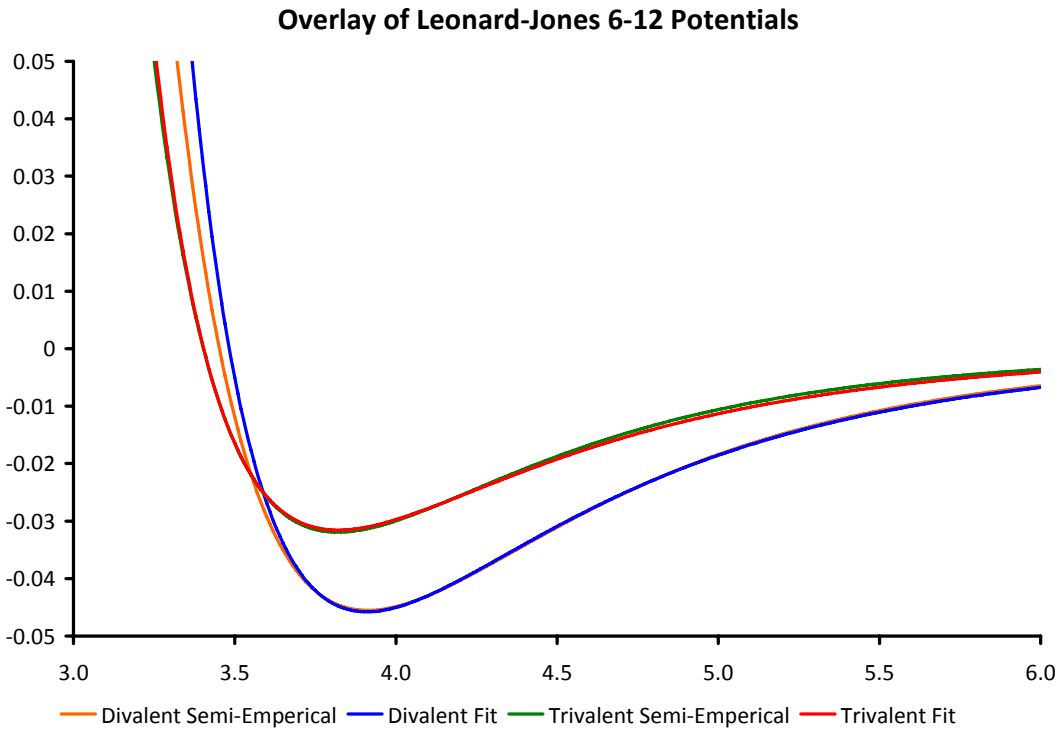

Figure 5. Comparison of the potential energy fit between the semi-empirical expression of Curtiss et al. (1987) as reported by Guàrdia and Padró (1990) and the Lennard-Jones parameters for: divalent (Fe^{2+}) and trivalent (Fe^{3+}) iron.

Then a molecular dynamics simulation was performed with a canonical ensemble (*NVT*) over 750 ps at 298K applying the Nosé-Hoover thermostat. Each siderophore configuration was also paired with each of the metal cations. For each siderophore-cation pair, the energy of the system was minimized and then a molecular dynamics simulation was performed with a canonical ensemble (*NVT*) over 750 ps at 298K applying the Nosé-Hoover thermostat. The average total energy and potential energy were calculated for each of the nine siderophore configurations and for the 27 unique siderophore-cation pairs. In addition, the structure of each siderophore configuration and metal-ligand complex was examined.

Table 2. Metal Ion Force Field Parameters

Metal Ion	q	σ	ε
Fe(II) 2.0		2.6250	1.3650
Fe(III) 3.0		2.4110	1.9798
UO_2(VI) 2.5		2.8315	0.3733

3.0 RESULTS

3.1 Siderophore Conformations

The final trajectory frame of each MD simulation for the nine siderophore configurations is depicted in Figure 6. There are three siderophore configurations with a neutral charge. These are called DFO-B 0A, 0B, and 0C, where the A acetohydroxamate group is nearest the terminal amine group and C is the furthest. The group specified in the name (e.g., A, B, or C), is the deprotonated acetohydroxamate group. There are also three siderophore configurations in which DFO-B has a -1 charge. These are called DFO-B -1 AB, -1 AC, and -1 BC, where again the letters A, B, and C indicate the deprotonated acetohydroxamate groups in the configuration. For each of the additional charge states, +1, -2, and -3, there is only one siderophore configuration.

Several distances are marked on each configuration illustrated in Figure 6. In each configuration with NH_3^+, the amine group is hydrogen bonded to one of the oxygen atoms in the siderophore. This oxygen atom can be part of a protonated or deprotonated acetohydroxamate group; or part of an acetylamine group. The only configuration with an NH_2 group is the fully deprotonated DFO-B -3 is the only configuration with an NH_2 group. This group does not form a hydrogen bond with another part of the siderophore chain. The hydroxyl group frequently forms a hydrogen bond with the double-bonded oxygen of the same acetohydroxamate group. Figure 6 shows that with deprotonation, the acetohydroxamate oxygen atoms separate from each other. Finally, it should be noted that although all the configurations were constructed to have only *cis*-keto acetohydroxamate groups, in DFO-B -3, one of the groups has become *trans*. Additional simulations of different configurations would be necessary to determine if this change in conformers is necessary to form the lowest energy configuration.

The average potential energy calculated for each siderophore configuration during the MD simulations is provided in Table 3. There is no overall trend in system energy as a function of charge or protonation scheme. The size of the siderophore complex and the number of different torsion angles possible between the functional groups along the chain make it difficult to insure that the lowest energy configurations were simulated. The energy reported in Table 3 for DFO-B 0C is very different from those reported for DFO-B 0A and for DFO-B 0B. More simulations would be necessary to determine if there is a stable DFO-B 0C configuration with a lower potential energy similar to those reported for DFO-B 0A and DFO-B 0B. The best that we can say is that each siderophore configuration represents a local minimum energy structure. The Several different approaches such as umbrella sampling of numerous starting configurations, increasing the simulation time or temperature, or potential of mean force calculations could be used to improve upon these preliminary, screening calculations.

Table 3. Average Potential Energy for Each Siderophore from MD Simulation (kcal/mol)

	DFO-B +1	DFO-B 0A	DFO-B 0B	DFO-B 0C	DFO-B -1AB	DFO-B -1AC	DFO-B -1BC	DFO-B -2	DFO-B -3
PE	41.46	-43.12 -4	2.47	53.18	-21.12 -2	6.07	44.02	-21.59 -2	6.07

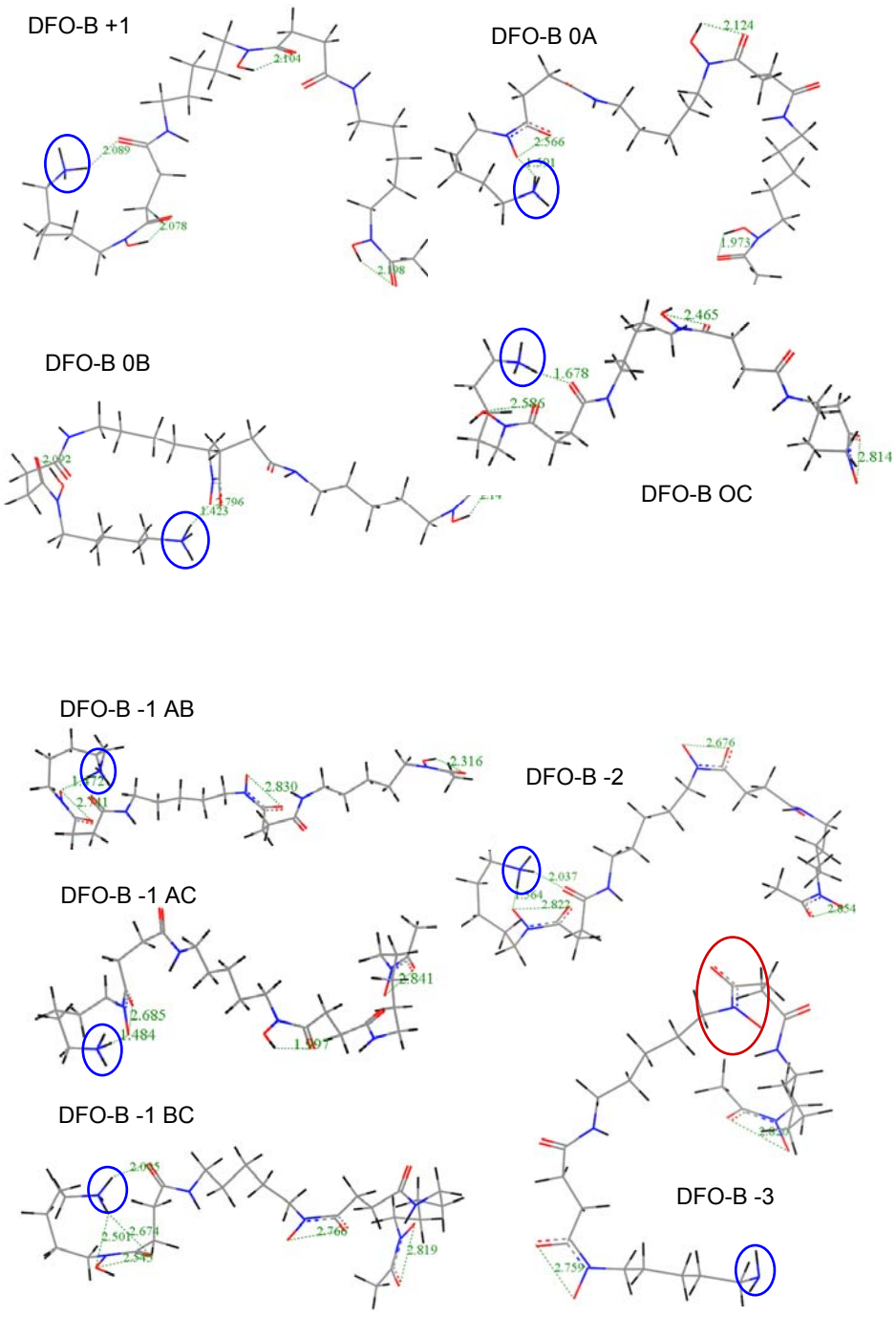

Figure 6. DFO-B in different charge and structural configurations. The blue circles indicate the terminal amine group. The red circle indicates a *trans*-acetohydroxamate group. The green dotted lines and numbers indicate atomic distances.

3.2 Complexing of siderophores with Fe(II)

Adding a cation to the pre-equilibrated siderophore configurations described in Section 3.1 did not lead to fully chelated structures upon geometry optimization and a 750 ps molecular simulation time. Instead the cation binds to one or two of the functional groups available on the siderophore chain. Molecular dynamics simulations at increased temperature (e.g., 600K) resulted in more chelation, but still did not lead to the expected minimum potential energy configurations with chelation to all three acetohydroxamate groups. Therefore, the model siderophore was initially wrapped around the cation prior to geometry optimization and simulation. In all cases, the cation was greater than 4 Å away from any part of the siderophore prior to performing any calculation. A comparison between the average potential energy calculated in the "annealed" simulations and those started with the acetohydroxamate groups favorably oriented toward the cation showed that the latter starting configurations achieved lower system energies. Again, because of the bulky nature of the siderophore, and a constraint on the number of simulations we could perform, we are not assured of achieving the lowest energy structure in all cases.

Figure 7 illustrates the coordination of Fe(II) to six of the nine siderophore configurations. These figures correspond to the final snapshot of the simulation and represent typical configurations that occur during the 750 ps timeframe. Siderophore oxygen atoms are considered to be involved in chelation if they are < 3.0 Å away from Fe(II). The majority of the simulated configurations exhibit six-fold Fe(II) coordination. However, under conditions in which one or more of the acetohydroxamate groups is protonated, the six oxygen atoms of these three groups are not all involved in chelation. Instead, one or more oxygen atoms from the acetylamine (-CC(O)NC-) groups in the polymer chain are involved in Fe(II) chelation. The configuration shown for DFO-B 0C exhibits four-fold Fe(II) coordination with two bonds from the deprotonated acetohydroxamate group, one bond to the doubly-bonded oxygen atom of a protonated acetohydroxymate group, and one bond with the oxygen atom of an acetylamine group. The unique nature of this coordination scheme suggests that additional simulations should be performed with different starting configurations to determine if this scheme represents the lowest energy state.

For the DFO-B in the -2 and -3 charge states, all three hydroxamate groups are deprotonated, and Fe(II) chelation occurs as expected with the six oxygen atoms of the acetohydroxamate groups.

3.3 Complexing of siderophores with Fe(III)

Again, for Fe(III), the model siderophore was initially wrapped around the cation prior to geometry optimization and simulation. In all cases, the cation was not within a 4 Å distance to any part of the siderophore prior to energy minimization. The coordination for Fe(III) with the siderophore varies between six and seven. Chelation is again defined by oxygen-Fe distances of < 3 Å. The chelated structures for the nine DFO-B structures with Fe(III) are illustrated in Figure 8. For DFO-B +1, the doubly-bonded oxygen atoms of each acetohydroxamate group is involved in Fe(III) chelation. The middle or B acetohydroxamate group of the siderophore chain has rotated from the *cis* to *trans* configuration. Two oxygen atoms from acetylamine groups of

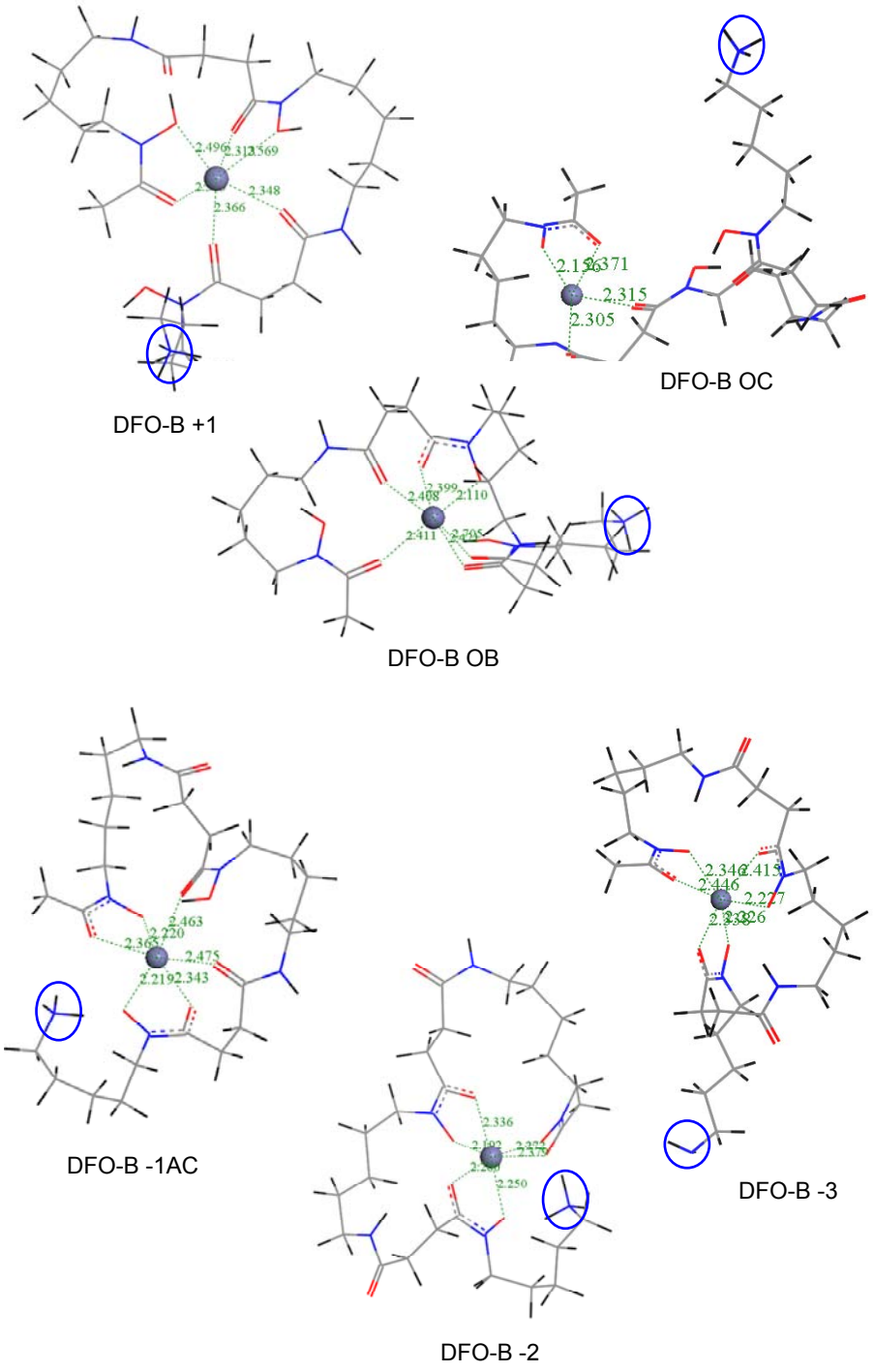

Figure 7. Fe(II) chelation to different DFO-B charge and structural configurations. The blue circles indicate the terminal amine group. The green dotted lines and numbers indicate atomic distances.

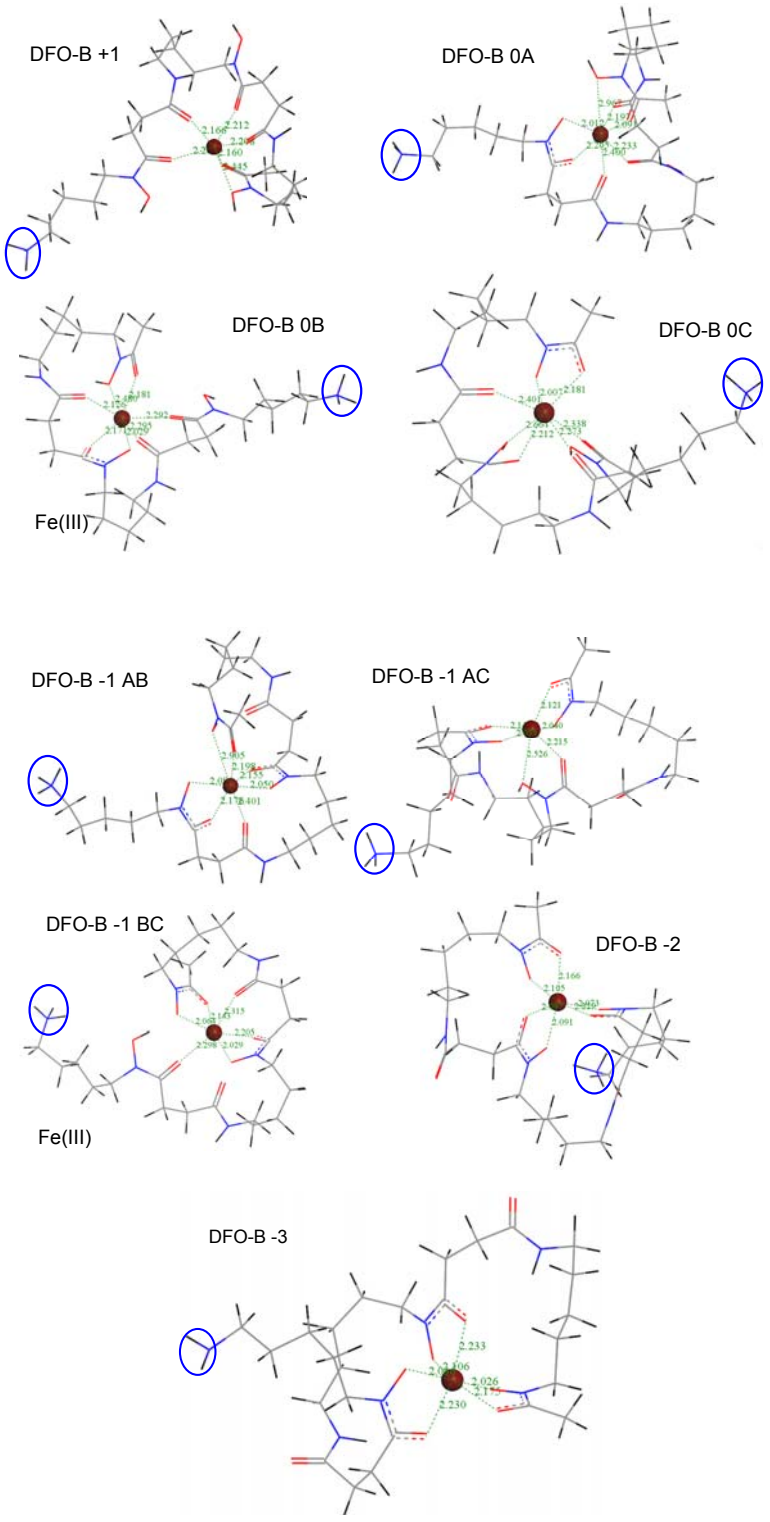

Figure 8. Fe(III) chelation to different DFO-B charge and structural configurations. The blue circles indicate the terminal amine group. The green dotted lines and numbers indicate atomic distances.

the siderophore chain are also involved in Fe(III) chelation. The sixth oxygen atom chelating Fe(III) is part of the C acetohydroxamate group.

The three neutral siderophore structures, DFO-B 0A, 0B, and 0C all exhibit seven-fold coordination with Fe(III). In all three cases, both oxygen atoms from the deprotonated acetohydroxamate group, and the two doubly-bonded oxygen atoms of the other acetohydroxamate groups are involved in Fe(III) chelation. In 0A and 0B, one of the hydroxyl oxygens is involved in chelation; however, in 0C, both of the hydroxyl oxygens from the acetohydroxamate groups are involved in chelation. One or two oxygen atoms from the acetylamine groups are also involved in chelation in each of these configurations.

DFO-B -1 AB also exhibits seven-fold coordination with Fe(III): all six of the oxygen atoms in the acetohydroxamate groups bind to Fe(III), as well as one doubly-bonded oxygen atom from an acetylamine group. In our simulations, DFO-B -1 AC forms six bonds with Fe(III) through the three acetohydroxamate groups. In contrast, the hydroxyl oxygen in DFO-B -1 BC does not form a bond with Fe(III). Instead, another acetylamine group bonds to the cation. For DFO-B -2 and DFO-B -3, the expected six-fold coordination to the oxygen atoms of the deprotonated acetohydroxamate groups is simulated.

3.4 Complexing of siderophores with UO_2(VI)

For UO_2(VI), the initial siderophore-UO_2(VI) configuration was again arranged so that chelation between the acetohydroxamate groups and the metal cation could conveniently occur. For this set of simulations, UO_2(VI) was substituted for Fe(III) in the initial configurations used for the simulations discussed in Section 3.3. Again, the uranyl cation was initially over 4 Å from the siderophore prior to energy minimization. The coordination for UO_2(VI) with the siderophore varies between four and six, where distances of < 3 Å between the uranium atom of the uranyl cation and the siderophore-oxygen are assumed to indicate a bond. The chelated structures for the nine simulated uranyl-DFO-B structures are illustrated in Figure 9. For DFO-B +1, only the double-bonded oxygens of the three acetohydroxamate groups and of the two acetylamine groups participate in chelating the uranyl cation to the siderophore. DFO-B 0A and DFO-B 0B both form five bonds with the uranyl cation; two with the oxygens of the deprotonated acetohydroxamate group. For DFO-B 0A, three more bonds are formed with the double-bonded oxygen atoms of the protonated acetohydroxamate groups and with one of the acetlyamine groups. For DFO-B 0B, three more bonds are made with the two oxygen atoms of a protonated acetohydroxamate group and the oxygen atom of an acetylamine group. DFO-B 0C forms only four bonds with uranyl with both oxygen atoms of the deprotonated acetohydroxamate group (Group C), the double-bonded oxygen of Group B, and the double-bonded oxygen of the acetylamine group in between Groups B and C.

Siderophores DFO-B AB, AC, and BC each with a charge of -1, also form four or five bonds with UO_2(VI). For each metal-ligand structure, the four oxygen atoms of the two deprotonated acetohydroxamate groups are involved in chelation. The doubly-bonded oxygen atom of the third acetohydroxamate group in DFO-B AB and DFO-B BC forms a fifth bond with the uranyl cation. Uranyl forms five bonds with DFO-B -2 and six bonds with DFO-B -3. In both structures, only the acetohydroxymate groups are involved in chelation. For DFO-B -2, Figure 9 also shows that the terminal amine group NH_3^+ forms hydrogen bonds with two of the

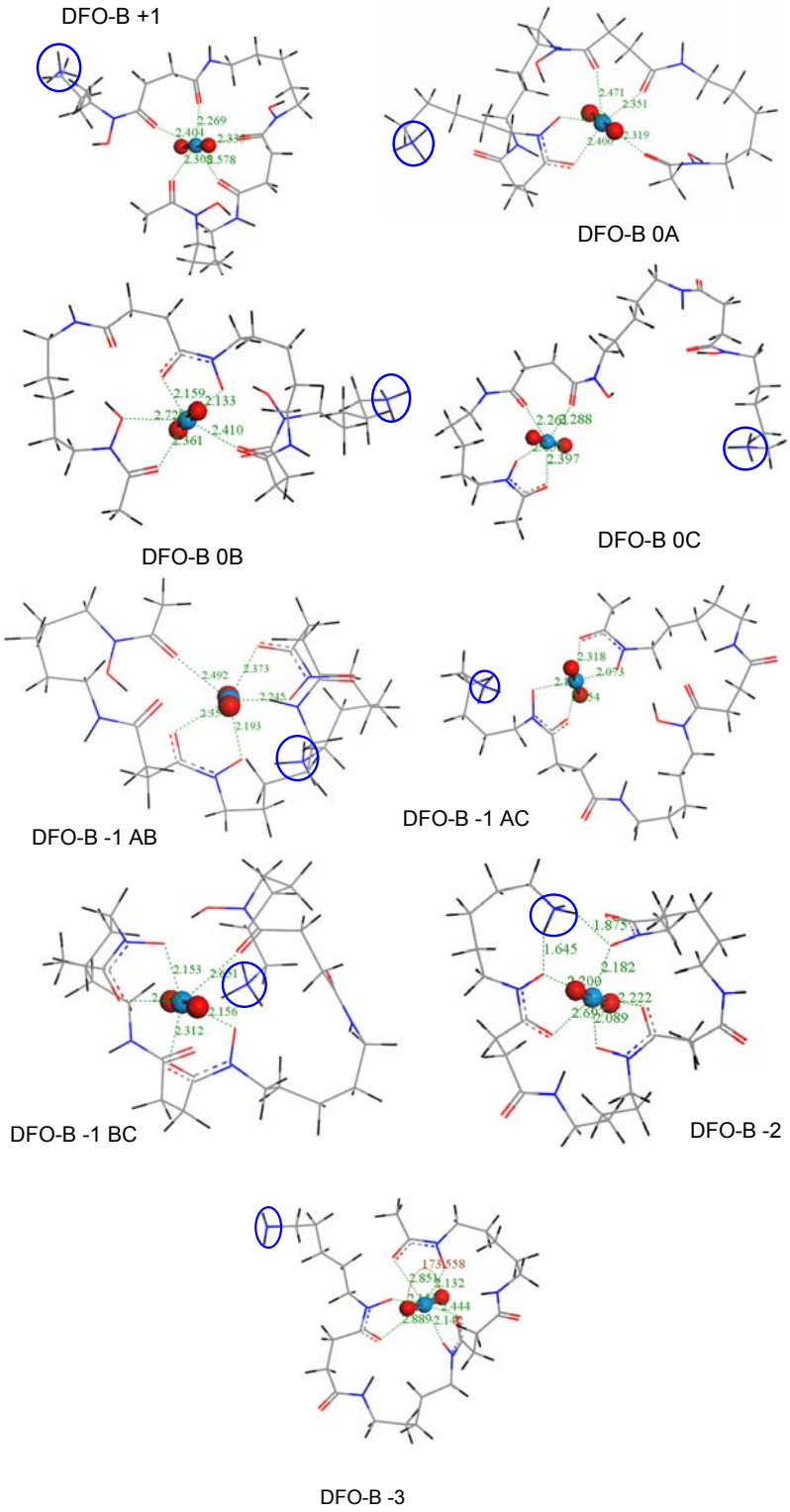

Figure 9. UO_2(VI) chelation to DFO-B in different charge and structural configurations. The blue circles indicate the terminal amine group. The red circle indicates a *trans*-acetohydroxamate group. The green dotted lines and numbers indicate atomic distances.

hydroxymate groups of the siderophore, while the NH_2 group in DFO-B -3 points away from the acetohydroxamate groups.

3.5 Potential Energy

Figure 10 illustrates the potential energy for each simulated siderophore-metal complex. The trend from left to right on the abscissa is roughly correlated with solution pH – going from the most acidic (Sid+1) to the most basic (Sid-3). For each siderophore configuration, Fe(III) forms the most favored complex. The uranyl complexes have slightly lower potential energy than the Fe(II) complexes. These initial results suggest that under anaerobic conditions, uranyl complexation may be preferable to iron complexation. However, under aerobic conditions, DFO-B will select for Fe(III) over uranyl. The similarity between the potential energy for Fe(II) and UO_2(VI)-siderophore complexes suggests that Coulombic energy plays a dominant role in metal chelation. For all three cations, stronger metal-siderophore complexation occurs with the negatively-charged siderophores. The most energetically stable complexes are formed with DFO-B -2, even for Fe(III). This result emphasizes that the terminal amine group does not play a role in metal chelation. Figure 10 also illustrates that the system potential energy for Fe(II) interaction with each of the three neutral siderophores is roughly equilivalent. The same is true for Fe(II) binding to each of the (-1) siderophores. Potential energies for siderophore-Fe(III) and siderophore-UO_2(VI) complexes also exhibit little difference between siderophores of the same charge but different protonation schemes.

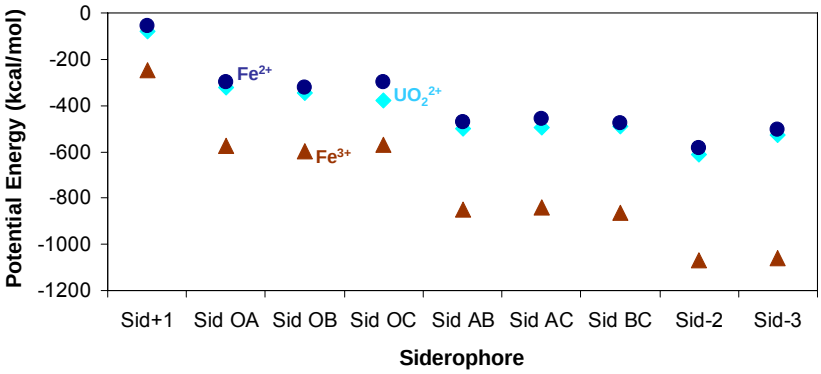

Figure 10. Potential Energy of Siderophore-Metal Complexes in Vacuum

4. CONCLUSIONS

In summary, several observations can be made from our molecular dynamics simulations for DFO-B with Fe(II), Fe(III), and UO_2(VI). First, as would be expected, the number of bonds involved in metal chelation decreases with increasing metal ion size. The ionic radii for Fe(III), Fe(II), and U(VI) are 0.69 Å, 0.76 Å, and 0.90 Å, respectively. The calculated coordination number for Fe(III) to DFO-B is either 6 or 7, for Fe(II) the calculated number is usually 6, and for UO_2(VI), the calculated coordination number is often 5. Although both the Fe(III) and UO_2(VI) simulations were performed with approximately the same starting configurations, the functional groups binding to UO_2(VI) for each siderophore structure are not always a subset of the functional groups that bind to Fe(III). This difference could be dependent on the orientation of UO_2(VI) with respect to the siderophore or related to the overall size of the multi-atom cation. More simulations would be required to understand this discrepancy in more detail.

The calculated metal-siderophore potential energies are consistent with measured association constants, indicating that the trend in metal-siderophore stability is Fe(II) < UO_2(VI) < Fe(III). It is worth noting that this sequence is not correlated with ionic radii, but may be more affected by ion charge. Despite the fact that we did not do a systematic analysis of how different rotations and torsions of the siderophore might impact the total binding energy, the similarity in the calculated potential energies for each charge state, suggests that the Coulombic energy term is much larger than those associated with different polymer morphologies.

Although metal-siderophore association constants are reported for various DFO-B species, the structure of the metal-siderophore complexes for protonated DFO-B structures has never been reported. This is the first time that involvement of the acetylamine groups in metal-binding has been proposed. Previous studies have focused only on the chelation between the deprotonated acetohydroxamate groups and a metal cation. While this is clearly the most stable structure formed, it will only form over a limited pH range, from pH 9 to 10. Most natural waters are less alkaline than pH 9; therefore the other siderophore-metal structures may be more prevalent in the environment. In addition, this study showed that the DFO-B -2 formed the most stable structures with the various metal cations, including Fe(III). This result suggests that the location of charge along the polymer chain and the nature of the charged functional groups plays a role in metal binding to siderophores.

Future work should include simulating metal binding to DFO-B and other biologically-designed siderophores in aqueous solution as well as in vacuum. These chelators exhibit higher association constants for Pu(IV) than for Fe(III) (See Table 1) and should readily remove Pu(IV) from various waste streams. In addition, these siderophores show promise for extracting Th(IV), and UO_2(VI) from aqueous solutions that have low Fe(III) concentations. Because the deprotonated siderophores may only exist in alkaline solutions, the structure and metal-binding potential of protonated siderophores should also be studied. Molecular simulation allows for detailed understanding of metal binding to these organic chelators and a better appreciation for the complexity of bacterial interaction with the environment.

5. REFERENCES

Accelyrs Inc., San Diego. Materials Studio, Forcite Module.

Berendsen, H. J. C., Postma, J. P. M., van Gunsteren, W. F., and Hermans, J., 1981. Interaction models for water in relation to protein hydration. In: Pullman, B. (Ed.), *Intermolecular Forces*. D. Reidel.

Boukhalfa, H. and Crumbliss, A. L., 2002. Chemical aspects of siderophore mediated iron transport. *BioMetals* **15**, 325-339.

Boukhalfa, H., Reilly, S. D., and Neu, M. P., 2007. Complexation of Pu(IV) with the Natural Siderophore Desfierrioxamine B and the Redox Properties of Pu(IV)(siderophore) Complexes. *Inorganic Chemistry* **46**, 1018-1026.

Curtiss, L. A., Halley, J. W., Hautman, J., and Rahman, A., 1987. Nonadditivity of ab-initio pair potentials for molecular dynamics of multivalent transition metal ions in water. *Journal of Chemical Physics* **86**, 2319-2327.

Dauber-Osguthorpe, P., Roberts, V. A., Osguthorpe, D. J., Wolff, J., Genest, M., and Hagler, A. T., 1988. Structure and Energetics of Ligand Binding to Proteins: *Escherichia coli* Dihydrofolate Reductase-Trimethoprim, A Drug-Receptor System. *PROTEINS: Structure, Function, and Genetics* **4**, 31-47.

Edwards, D. C., Nielsen, S. B., Jarzecki, A. A., Spiro, T. G., and Myneni, S. C. B., 2005. Experimental and theoretical vibrational spectroscopy studies of acetohydroxamic acid and desferrioxamine B in aqueous solution: Effects of pH and iron complexation. *Geochimica et Cosmochimica Acta* **69**, 3237-3248.

Evers, A., Hancock, R. D., Martell, A. E., and Motekaitis, R. J., 1989. Metal ion recognition in ligands with negatively charged oxygen donor groups. Complexation of Fe(III), Ga(III), In(III), Al(III), and other highly charged metal ions. *Inorganic Chemistry* **28**, 2189-2195.

Frazier, S. W., Kretzschmar, R., and Kraemer, S. M., 2005. Bacterial siderophores promote dissolution of UO_2 under reducing conditions. Environmental Sciences and Technology **39**, 5709-5715.

Guardia, E. and Padro, J. A., 1990. Molecular dynamics simulations of ferrous and ferric ions in water. *Chemical Physics* **144**, 353-362.

Guilbaud, P. and Wipff, G., 1996. Force field representation of the UO_2^{2+} cation from free energy MD simulations in water. Tests on its 18-crown-6 and NO_3^- adducts, and on its calix[6]arene6- and CMPO complexes. *Journal of Molecular Structure* **366**, 55-63.

Hernlem, B. J., Vane, L. M., and Sayles, G. D., 1996. Stability constants for complexes of the siderophore desferrioxamine B with selected heavy metal cations. *Inorganic Chimica Acta* **244**, 179-184.

Hernlem, B. J., Vane, L. M., and Sayles, G. D., 1999. The application of siderophores for metal recovery and waste remediation: Examination of correlations for prediction of metal affinities. *Water Research* **33**, 951-960.

Mullen, L., Gong, C. and Czerwinski, K., 2007. Complexation of uranium(VI) with the siderophore desferrioxamine B. *Journal of Radioanalytical and Nuclear Chemistry* **273**, 683-688.

Teleman, O., Jonsson, B., and Engstrom, S., 1987. A molecular dynamics simulation of a water model with intramolecular degrees of freedom. *Molecular Physics* **60**, 193-203.

Whisenhunt, D. W. J., Neu, M. P., Hou, Z., Xu, J., Hoffman, D. C., and Raymond, K. N., 1996. Specific sequestering agents for the actinides. 29. Stability of the Thorium(IV) complexes

of Desferrioxamine B (DFO) and three octadentate catecholate or hydroxypyridinonate DFO derivatives: DFOMTA, DFOCAMC, and DFO-1,2-HOPO. Comparative stability of the Plutonium(IV) DFOMTA complex. *Inorganic Chemistry* **35**, 4128-4136.

DISTRIBUTION

EXTERNAL DISTRIBUTION

Everett Shock
Department of Geological Sciences
Arizona State University
P.O. Box 871404
Tem pe, Arizona 85287-1404

Jason Raymond
University of California, Merced
School of Natural Sciences
P.O. Box 2093
Merced, California 95344

INTERNAL DISTRIBUTION

1	MS0735	John Merson	06310
1	MS0754	Susan Altman	06316
1	MS0754	Patrick V. Brady	06310
5	MS0754	Louise J. Criscenti	06316
1	MS0754	Randall T. Cygan	06316
1	MS0754	Jeffery A. Greathouse	06316
2	MS0754	Nathan Ockwig	06316
1	MS0754	May Nyman	06316
1	MS0754	James L. Krumhansl	06316
1	MS0754	Mark Rigali	06316
1	MS0776	Kathyren B. Helean	06781
1	MS0776	Yifeng Wang	06781
1	MS0779	Kathleen C. Holt-Larese	06772
1	MS0886	Todd M. Alam	01816
1	MS0886	James A. Voigt	01816
1	MS1104	Rush D. Robinett III	06300
1	MS1104	Margerie L. Tatro	06200
1	MS1303	George Bachand	01332
1	MS1349	Jeffrey C. Brinker	01002
1	MS1395	Ahmed Ishmail	06711
1	MS1411	Eric Spoerke	01411
1	MS1413	Grant Heffelfinger	08630
1	MS0899	Technical Library	09536
1	MS0123	D. Chavez, LDRD Office	01011


Sandia National Laboratories